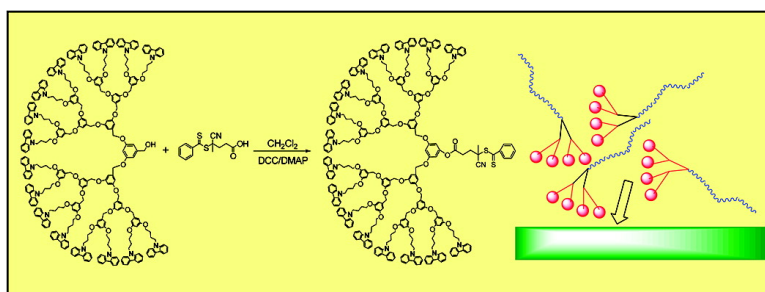# Macromolecules

Article

Electrochemically Active Dendritic#Linear Block Copolymers via RAFT Polymerization: Synthesis, Characterization, and Electrodeposition Properties

Derek L. Patton, Prasad Taranekar, Timothy Fulghum, and Rigoberto Advincula

More About This Article

Additional resources and features associated with this article are available within the HTML version:

- Supporting Information
- Access to high resolution figures
- Links to articles and content related to this article
- Copyright permission to reproduce figures and/or text from this article

View the Full Text HTML

Electrochemically Active Dendritic−Linear Block Copolymers via RAFT Polymerization: Synthesis, Characterization, and Electrodeposition Properties

Derek L. Patton,[†] **Prasad Taranekar, Timothy Fulghum, and Rigoberto Advincula***

Department of Chemistry and Department of Chemical and Biomolecular Engineering, University of Houston, Houston, Texas 77204

Received March 22, 2008; Revised Manuscript Received July 6, 2008

ABSTRACT: We describe a series of well-defined dendritic−linear block copolymer architectures via the reversible addition−fragmentation chain transfer (RAFT) polymerization technique. Using dendritic chain transfer agents (CTA)s possessing a single dithioester moiety at the focal point, RAFT polymerization was carried out to attach polystyrene (PS) and poly(methyl methacrylate) (PMMA) chains of controlled lengths by kinetic control. To provide electrochemical functionality, the dendritic CTAs were designed with carbazole moieties at the periphery of the structures. The results on the electrochemical polymerization of the carbazole moieties at the periphery of the dendritic component of the block copolymers reveal quantitative cyclic depositions with changes in viscoelastic properties of the deposited films as monitored by the electrochemical quartz crystal microbalance technique. The electroactive dendritic blocks proved to be an effective electrochemically active macromonomer for the electrodeposition of these structures on conducting substrates.

Introduction

Dendrimers and dendrons are a unique class of macromolecules that exhibit monodisperse molecular weight, high degree of surface functionality, and well-defined branched architectures emanating from a central focal point.[1] Some possible applications have included light-harvesting materials,[2] drug delivery,[3] and catalysis.[4] Furthermore, the modification of dendritic structures at both the focal point[5] and the periphery[6−8] has greatly improved the versatility and applicability to other macromolecular systems. In particular, the combination of dendritic and linear segments shows great promise as a functional class of block copolymers.[9−17] These dendritic−linear block copolymers offer the opportunity to combine the unique interfacial properties and high functionality of dendrimers with the phase separation behavior and processability of linear polymers. A number of solid-state morphological studies have recently been reported in which the dendritic−linear block copolymers have been shown to self-assemble into a wide range of microphase-separated domains including lamella, rods, and spheres.[13,18−22] The specific morphologies adopted by the various systems mentioned above were dictated by factors including volume fraction, generation number of the dendron, and the molecular weight of the linear chain. Interesting behavior of the dendritic−linear hybrids has also been observed under dilute solution conditions.[14,22,23] For example, Passeno et al. observed a conformational change of both the linear (knitted to random coil) and dendritic block (spherical to cone) as a function of linear molecular weight.[24]

A number of different synthetic strategies have been recently developed. One strategy involves coupling of preformed end-functionalized linear polymers with reactive dendritic architectures having a complementary functional group at their focal point. This approach was employed by Gitsov and co-workers to produce dendritic−linear block copolymers by the reaction of hydroxyl-terminated poly(ethylene glycol) and poly(ethylene oxide) with bromobenzyl-functionalized aromatic polyether dendrons using Williamson etherification.[10,22,25] Alternatively, similar dendritic−

linear copolymers were obtained by the termination of anionic polystyrene with polyether dendrons.[26] Although this strategy yields the block copolymer in one step, it is limited by the availability of macromolecular systems with appropriate coupling chemistries. Another approach to dendritic−linear block copolymers involves a divergent synthetic strategy of the dendron segment from an appropriately end-functionalized linear polymer.[12,27] Namazi et al. used such an approach in the synthesis of ABA dendritic triazine−linear poly(ethylene glycol) block copolymers.[28] A more promising approach to dendritic−linear block copolymers was first demonstrated by Gitzov and co-workers in which dendrons were used as macroinitiators in the anionic polymerization of ε-caprolactone.[29] Al-Muallem et al. extended this approach with a one-pot synthesis of dendritic−linear polystyrene derivatives by a convergent-like living anionic synthesis of dendritic polystyrene followed by the growth of the linear polystyrene segment.[30,31] The down side of the aforementioned examples lies in the stringent conditions associated with anionic polymerization. In contrast, controlled radical polymerization (CRP) techniques—such as nitroxide-mediated polymerization (NMP), atom transfer radical polymerization (ATRP),[32] and reversible addition−fragmentation chain transfer polymerization (RAFT)[33,34]—offer an unparalleled opportunity for the rational design and control of macromolecular architectures under milder reaction conditions. Dendritic macroinitiators have been combined with CRP techniques such as NMP and ATRP. Leduc and co-workers first reported the use of poly(aryl ether) dendrons possessing a single benzylic TEMPO or halide functionality at the focal point of the dendron for NMP and ATRP, respectively.[13,35] A number of other groups have used similar synthetic strategies in the design of well-defined dendritic−linear systems consisting of various linear copolymer compositions.[17,36,37] To our knowledge, the combination of dendritic focal point chain transfer agents and RAFT polymerization has been rarely reported as a route to dendritic−linear block copolymer systems.[38] The inherent stability and chemical versatility of chain transfer agents (CTAs) utilized in the RAFT technique allow the preparation of well-defined polymers with specific polymer architectures and end-group functionalities. However, until now, dendrimers have only been used as scaffolds for RAFT CTAs at the periphery of the

* Corresponding author. E-mail: radvincula@uh.edu.
† Current address: School of Polymers and High Performance Materials, University of Southern Mississippi, Hattiesburg, MS 39406.
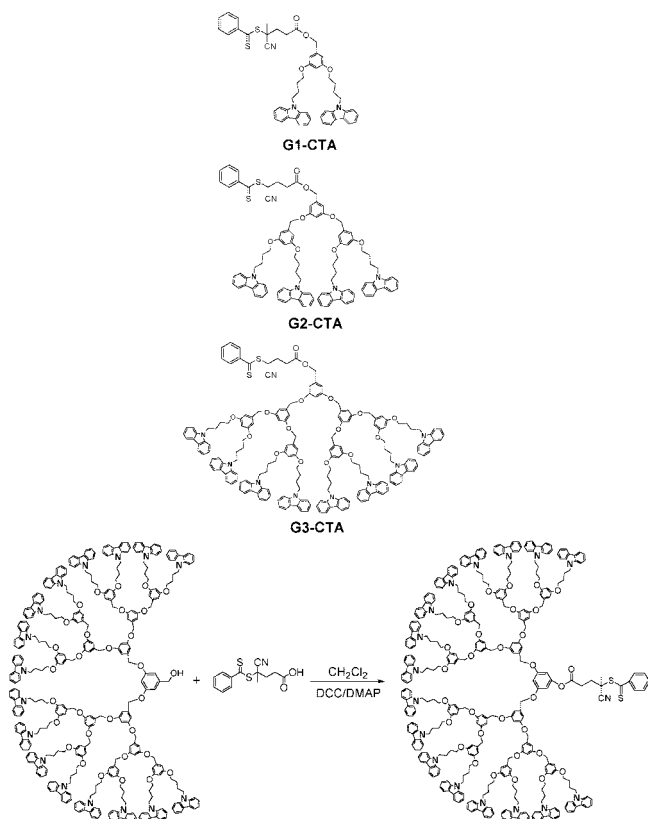
Figure 1. Synthesis of the G1-, G2-, G3-, and G4-Cbz-CTAs.

dendrons, thus leading to multiarm or star-shaped block copolymers.[39−41]

The incorporation of electro-optical properties in dendritic−linear block copolymer architectures is an attractive challenge to demonstrate utility of these complex systems. These properties can be included in the linear or dendritic blocks. In particular, we are interested in structures that possess electropolymerizability in conducting substrates and surfaces. Our group has previously demonstrated the "precursor polymer" approach as a route to conjugated polymer networks.[42−44] We have investigated several carbazole-containing "precursor polymers", some of which have shown improved hole transport properties in light-emitting diode devices.[45,46] Therefore, the incorporation of the "precursor polymer" approach into more complex macromolecular architectures is an important direction toward their wide applicability in ultrathin film formation and electro-optical functionality.

In this work, we describe the use of a series of functional dendritic CTAs for the preparation of well-defined hybrid dendritic−linear polymer architectures via the RAFT polymerization technique. A series of dendritic CTAs were first synthesized possessing a single dithioester moiety at the focal point of the dendron, culminating with a fourth generation CTA dendron, G4-Cbz-CTA (Figure 1). We believe that this work is one of the first report on the synthesis of electrochemically active linear−dendron block copolymers capable of electrodeposition on conducting surfaces. This work also presents a comparative and exploratory kinetic study to establish appropriate reaction conditions for a variety of monomers in the presence of the functional CTAs. As an example of electrochemical functionality, the dendritic CTAs were designed with carbazole moieties at the periphery of the structures. In addition, we present the preliminary results on the electrochemical polymerization of the carbazole moieties at the periphery of the dendritic component of the block copolymers. The electro-active dendritic block proved to be an effective electrochemically active macromono-

mer for the electrochemical deposition of these structures on conducting substrates.

Experimental Section

Materials. Reagent chemicals were purchased from Aldrich and used without further purification unless otherwise indicated. Tetrahydrofuran (THF) used in synthesis was distilled from sodium/benzophenone ketyl. Styrene (99+%), methyl methacrylate (MMA, 99+%), and methyl acrylate (MA, 99%) were passed through a column of activated basic alumina to remove the inhibitor, distilled, and stored at −20 °C. 2,2′-Azobis(isobutyronitrile) (AIBN) was recrystallized twice from ethanol and stored at 5 °C in an amber bottle. Dithiobenzoic acid (DTBA)/sodium dithiobenzoate was prepared and subsequently oxidized to bis(thiobenzoyl)disulfide according to the literature.[47] 4-Cyano-4-((thiobenzoyl)sulfanyl)-pentanoic acid (**1**) was prepared as previously reported.[48]

Synthesis of G*n*-Cbz-OH (*n* = 1−4). The carbazole-functionalized dendrons with hydroxy focal points were synthesized according to the literature and have been previously reported.[49] The NMR of these compounds is given in the Supporting Information.

Synthesis of G4-Cbz-CTA. A solution of G4-Cbz-OH (0.78 g, 0.144 mmol), compound **1** (40.1 mg, 0.144 mmol), and 4-(dimethylamino)pyridine (DMAP) (2.5 mg, 0.02 mmol) was dissolved in anhydrous dichloromethane (15 mL) under N_2. Dicyclohexylcarbodiimide (DCC) (41.2 mg, 0.2 mmol) in 5 mL of DCM was added dropwise to the reaction mixture at 0 °C. The reaction was stirred vigorously at 0 °C for 5 min and then warmed to room temperature and stirred overnight. The reaction mixture was filtered to remove the white solid byproduct. The organic phase was washed with dilute $NaHCO_3$ and dried over anhydrous Na_2SO_4, and the solvent was removed under vacuum. The crude product mixture was first washed with ethyl acetate and then purified by column chromatography on silica gel with dichloromethane:hexane (4:1, v/v). The solvent was removed by rotary evaporation to yield G4-Cbz-CTA as a pink-orange solid (0.26 g, 32%). ^{1}H NMR (CDCl$_3$) δ (ppm): 8.03 (d, 32H); 7.77 (d, 2H); 7.42−7.14 (m, 99H); 6.70−6.40 (m, 37H); 6.25 (b, 8H); 5.00 (s, 2H); 4.85 (b, 28H); 4.25 (t, 32H,); 3.76 (t, 32H); 2.72−2.22 (m, 4H); 2.06−2.81 (m, 32H); 1.81−1.6 (m, 35H). ^{13}C NMR (CDCl$_3$) δ (ppm): 24.5, 26.4, 27.2, 29.9, 33.7, 43.4, 46.3, 60.9, 68.1, 70.6, 101.48, 106.5, 107.6, 109.2, 119.4, 120.9, 123.4, 126.2, 127.2, 129.1, 133.7, 139.6, 140.9, 160.6, 160.8, 171.98, 222.8.

Synthesis of G3-Cbz-CTA. G3-Cbz-CTA was prepared in a similar manner to G4-Cbz-CTA. The crude product mixture was first washed with ethyl acetate and then purified by column chromatography on silica gel with dichloromethane:hexane (4:1, v/v). The solvent was removed by rotary evaporation to yield G3-Cbz-CTA as a pink-orange solid (0.4 g, 60%). ^{1}H NMR (CDCl$_3$) δ (ppm): 8.10 (d, 16H); 7.81 (d, 2H); 7.50−7.18 (m, 51H); 6.70−6.48 (m, 17H); 6.31 (b, 4H); 5.04 (s, 2H); 4.92 (b, 14H); 4.32 (t, 16H,); 3.85 (t, 16H); 2.76−2.22 (m, 4H); 2.11−1.91 (m, 16H); 1.85−1.66 (m, 19H). ^{13}C NMR (CDCl$_3$) δ (ppm): 24.4, 26.4, 27.5, 29.9, 33.6, 43.2, 46.3, 60.9, 68.1, 70.6, 101.48, 106.5, 107.6, 109.2, 119.4, 120.9, 123.4, 126.2, 127.2, 129.1, 133.7, 139.6, 140.9, 160.6, 160.8, 171.98, 222.8.

Synthesis of G2-Cbz-CTA. G2-Cbz-CTA was prepared in a similar manner to G4-Cbz-CTA. The crude product was purified by column chromatography on silica gel with dichloromethane:hexane (4:1, v/v). The solvent was removed by rotary evaporation to yield G2-Cbz-CTA as a pink-orange solid (1.56 g, 68%). ^{1}H NMR (CDCl$_3$) δ (ppm): 8.11 (d, 8H); 7.88 (d, 2H); 7.58−7.19 (m, 27H); 6.64−6.49 (m, 7H); 6.34 (s, 2H); 5.08 (s, 2H); 4.94 (s, 4H); 4.37 (t, 8H,); 3.90 (t, 8H); 2.80−2.34 (m, 4H); 2.12−1.98 (m, 8H); 1.91−1.74 (m, 11H). ^{13}C NMR (CDCl$_3$) δ (ppm): 25.2, 26.4, 27.5, 35.5, 43.2, 56.3, 68.1, 70.6, 101.4, 106.4, 107.0, 107.7, 109.2, 119.4, 120.9, 123.4, 126.2, 127.2, 129.1, 133.5, 139.6, 140.9, 160.8, 171.8, 222.8.

Synthesis of G1-Cbz-CTA. G1-Cbz-CTA was prepared in a similar manner to G4-Cbz-CTA. The crude product was purified by column chromatography on silica gel with dichloromethane:

Table 1. Results and Conditions of the RAFT-Mediated Polymerization of Styrene in the Presence of the G*n*-Cbz-CTA Series

sample	CTA/polymer	time (h)	% conv^a	$M_{n,GPC}$ $(M_p)^b$	$M_{n,theory}^c$	PDI
1a	G1-Cbz-PS^d	2	5.80	3 346	3 864	1.06
1b		4	11.8	5 996	7 004	1.10
1c		8	20.3	11 603	11 426	1.15
1d		12	27.2	15 310	15 003	1.15
1e		24	41.3	23 527	22 351	1.22
2a	G2-Cbz-PS^e	2	13.2	6 963	8 410	1.08
2b		4	21.3	9 310	12 631	1.14
2c		8	35.2	16 197	19 867	1.19
2d		12	46.4	21 675	25 692	1.28
3a	G3-Cbz-PS^e	2	16.3	9 435	11 364	1.09
3b		4	24.1	15 229	15 437	1.14
3c		8	35.2	21 689	21 212	1.26
3d		12	44.9	27 665	26 289	1.29
4a	G4-Cbz-PS^f	1	14.0	8 929	20 202	1.17
4b		2	18.5	12 681	24 961	1.34
4c		4	31.5	22 302	39 365	1.65
4d		8	44.7	33 805	52 217	1.73

^{a} Conversion determined by monitoring the area under the RI curve for monomer and polymer in the crude reaction mixture. ^{b} Calculated using OmniSec software vs PS standards on purified samples. ^{c} $M_{n,theory}$ = [M]/[CTA] × conv × MW$_M$ + MW$_{CTA}$. ^{d} [M]:[CTA], 500:1; [CTA]:[I], 4:1; 70 °C. ^{e} [M]:[CTA], 500:1; [CTA]:[I], 3:1; 75 °C. ^{f} [M]:[CTA], 1000:1; [CTA]:[I], 3:1; 75 °C.

Table 2. Results and Conditions of the RAFT-Mediated Polymerization of Methyl Methacrylate in the Presence of the G*n*-Cbz-CTA Series

sample	CTA−polymer	time (h)	% conv^a	$M_{n,GPC}^b$	$M_{n,theory}^c$	PDI
5a	G1-Cbz-PMMA^d	1	5.66	6 708	4 244	1.25
5b		2	15.2	11 439	10 004	1.21
5c		4	25.9	17 624	16 413	1.28
5d		6	30.1	20 442	18 905	1.33
5e		8	34.2	23 214	21 363	1.38
6a	G2-Cbz-PMMA^e	0.5	14.5	9 032	10 258	1.21
6b		1	21.9	12 694	14 670	1.19
6c		2	35.1	18 526	22 596	1.26
6d		3	42.2	22 978	26 878	1.27
6e		4	52.0	26 400	32 765	1.29
7a	G3-Cbz-PMMA^e	0.5	15.2	8 092	12 064	1.18
7b		1	23.1	12 260	16 761	1.19
7c		2	36.3	17 369	24 708	1.29
7d		3	50.2	22 207	33 081	1.39
7e		4	59.5	24 642	38 650	1.41
8a	G4-Cbz-PMMA^f	0.5	9.10	14 886	14 762	1.36
8b		1	14.5	21 141	20 198	1.43
8c		2	27.5	31 018	33 222	1.53
8d		4	41.2	42 500	46 877	1.57
8e		8	52.6	48 857	58 310	1.63

^{a} Conversion determined by NMR of the crude reaction mixture. ^{b} Calculated using OmniSec software vs PS standards on purified samples. ^{c} $M_{n,theory}$ = [M]/[CTA] × conv × MW$_M$ + MW$_{CTA}$. ^{d} [M]:[CTA], 600:1; [CTA]:[I], 1.6:1; 70 °C ^{e} [M]:[CTA], 600:1; [CTA]:[I], 1.6:1; 80 °C. ^{f} [M]:[CTA], 1000:1; [CTA]:[I], 1.6:1; 75 °C.

hexane (4:1, v/v). The solvent was removed by rotary evaporation to yield G1-Cbz-CTA as a pink-orange solid (0.42 g, 70%). ^{1}H NMR (CDCl$_3$) δ (ppm): 8.13 (d, 4H); 7.88 (d, 2H); 7.6−7.24 (m, 15H); 6.48 (s, 2H); 6.37 (s, 1H); 5.08 (s, 2H); 4.40 (t, 4H,); 3.92 (t, 4H); 2.76−2.40 (m, 4H); 2.12−2.00 (m, 4H); 1.92−1.76 (m, 7H). ^{13}C NMR (CDCl$_3$) δ (ppm): 24.1, 25.9, 26.9, 29.8, 33.4, 42.7, 45.7, 66.8, 67.6, 101.2, 106.7, 108.6, 118.5, 118.9, 120.4, 122.9, 125.7, 126.7, 128.6, 133.0, 137.6, 140.4, 144.5, 160.2, 171.3, 222.3.

General Polymerization Procedure. All polymerizations were performed in a Schlenk apparatus under homogeneous conditions. The polymerizations were initiated by addition of AIBN. Solutions of the respective monomer, initiator, RAFT agent, and solvent were prepared in Schlenk tubes fitted with septa and a stir bar. The specific concentrations and conditions are noted in Tables 1 and 2. The mixtures were deoxygenated by 3−5 freeze−pump−thaw cycles, back-filled with nitrogen, and placed in a thermostated water bath at preset temperature. At specific time intervals, aliquots were

removed and quenched by lowering the temperature to 0 °C. The aliquots were used directly for GPC analysis. Purified polymer samples were obtained by repeated precipitation into methanol or hexane. In some cases, it was necessary to purify the polymer samples by passing through a short alumina column to remove the low molecular weight impurities. Further details are given in the discussions below. Monomer conversion was determined either by integration of the RI response for the crude monomer/polymer reaction mixture (styrene) or by ^{1}H NMR (methyl methacrylate).

Characterization. Gel permeation chromatography (GPC) was conducted on a Viscotek 270 (Viscotek, Inc.) equipped with an RI detector and a three-column series including 2 GMHHR-M and 1 GMHHR-L Mixed Bed ViscoGel columns. THF (Omnisolve, HPLC grade) served as the polymer solvent and eluent at a flow rate of 1 mL min^{-1}. Samples were prepared at a known concentration (ca. 1−3 mg/mL), and an injection volume of 100 μL was used. Monodisperse poly(styrene) and poly(methyl methacrylate) standards (EZ Vials, Polymer Laboratories) were used to construct the calibration curves. NMR spectra were recorded on a General Electric QE-300 spectrometer at 300 MHz for ^{1}H NMR and 75 MHz for ^{13}C NMR. FT-IR spectra were obtained on a Digilab FTS 7000 equipped with a HgCdTe detector at wavenumbers from 4000 to 600 cm^{-1} with a resolution of ∼8 cm^{-1}. FT-Raman spectra were recorded on the FTS 7000 spectrometer equipped with a germanium detector with the powder sample placed in separate capillary tubes. Excitation was provided by a Nd:YAG laser at a wavelength of 1064 nm, and the output laser power was 500 mW. The spectral resolution was ∼8 cm^{-1}, and 250 scans were collected for each sample. The thermal properties of the polymers were measured by thermogravimetric analysis (TGA) on a TA Instruments TGA 2920. The samples were heated up to 800 °C at a heating rate of 10 °C/min under a dry nitrogen atmosphere (flow rate: 80 mL/min) on a TA Instruments 2950 thermogravimetric analyzer. T_g was determined by DSC from the midpoint of the inflection tangent from the second heating at 5 °C/min. TGA and DSC data were analyzed using TA Instruments Universal Analysis software. The cyclic voltammetry (CV) experiments were carried out on a Princeton Applied Research Parstat 2263. For AFM analysis, an ITO substrate was used as the working electrode coupled with a Pt plate counter and Ag/AgCl reference electrode. Cyclic voltammetry was utilized to prepare films from a 2.0 mg/mL solution of the block copolymer solution in 0.1 M TBAH/CH$_2$Cl$_2$, where TBAH is tetrabutylammonium hexafluorophosphate.

Electrochemical quartz crystal microbalance (QCM) measurements were performed using an R-QCM (Maxtek Inc.) with an Amel 2049 potentiostat and Power laboratory system. The gold-coated QCM crystal was used as the working electrode, a Pt plate as the counter electrode, and Ag/AgCl reference electrode. The QCM apparatus, probe, and crystals are also available from Maxtek Inc. The diameter of the AT-cut polished QCM crystals (5 MHz) is 13 mm. The data acquisition was done with an R-QCM system equipped with a built-in phase lock oscillator and the R-QCM Data-Log software. The QCM crystals were cleaned with a oxygen/argon plasma etcher (Plasmod, March) immediately prior to use.

Results and Discussion

Synthesis and Characterization. *Synthesis of the Dendron RAFT Agents.* The dendritic CTAs were synthesized according to Figure 1 using the previously reported benzylhydroxy-terminated dendrons. These CTAs possess a single dithioester functional group at the focal point of the dendron allowing a straightforward RAFT approach to dendritic−linear block copolymers. We chose to incorporate the 4-cyano-4-((thiobenzoyl)sulfanyl)pentanoic acid functional group at the focal point of the dendrons for two reasons: (1) the 4-cyano-4-((thiobenzoyl)sulfanyl) portion of the molecule and its derivatives have proven to be an effective RAFT agent for styrene, methyl methacrylate, and a variety of other monomers,[50,51] and (2) the acid functionality facilitates a facile coupling to the dendrons containing a hydroxyl group at the focal point. In general, the
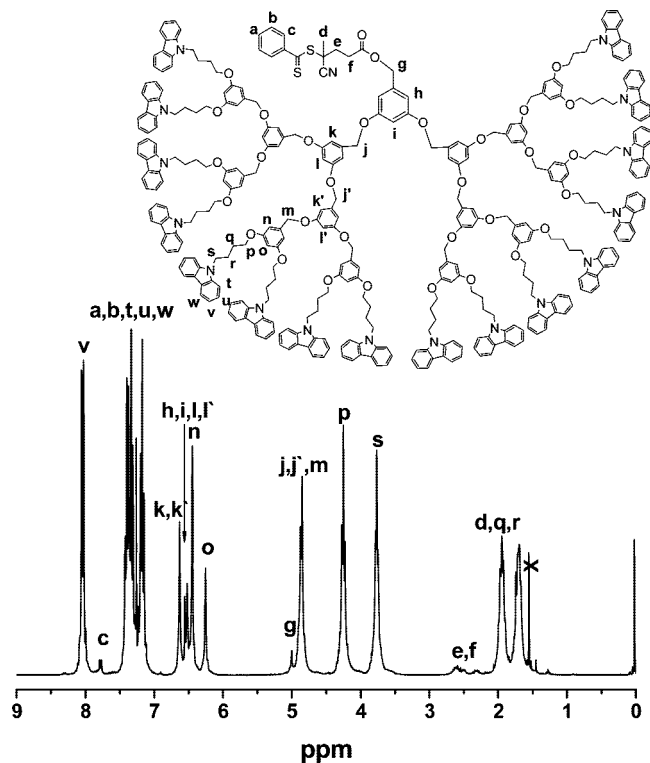
Figure 2. ^{1}H NMR spectrum of G4-Cbz-CTA.

Gn-Cbz-CTA (n = 1–4) series was prepared by the esterification of **1** and Gn-Cbz-OH in the presence of DCC/DMAP. The dendritic CTAs were obtained in decent yield after purification by column chromatography.

Figure 2 shows a typical ^{1}H NMR spectrum in the case of the G4-Cbz-CTA. The signals at δ = 7.87 (c) and at 2.34–2.74 ppm are attributed to the aromatic protons in the ortho position relative to the dithioester group and the two sets of methylene protons adjacent to the ester group, respectively. The signal at 5.05 ppm (g) is assigned to the benzylic protons of the dendron adjacent to the ester group (shifted downfield in comparison to the G3-Cbz-OH starting material) and is a good indication of a successful coupling reaction. The remaining protons of the G3-Cbz-CTA are fully assigned as shown in Figure 2. The characteristic bands for the series of dendritic CTAs were clearly observed by FTIR: C=S, 1048 cm^{-1}; C=O, 1736 cm^{-1}; C≡N, 2230 cm^{-1}. Further confirmation of the structure was obtained by FT-Raman spectroscopy (see Supporting Information Figure S1). The characteristic peaks of the dithioester portion of the molecule, namely the C≡N, C=S, and the C–S, were observed at 2227, 1248, and 645 cm^{-1}, respectively. In addition, the aromatic and aliphatic C–H stretches were respectively assigned at 3052, 2929, and 2874 cm^{-1}. The peaks at 1624, 1014, and 990 cm^{-1} were assigned to the in-plane ring-breathing mode of the aromatic ring. The peaks at 1593 and 1557 cm^{-1} are tentatively assigned to the C–C stretch of the aromatic ring of the benzene and carbazole units while the C=C stretch is located at 1312–1345 cm^{-1}.[52] Other assignments associated with the poly(aryl ether) dendritic structure include the –(O)CH$_2$ stretch (1457 cm^{-1}), the symmetric C–O–C stretch (842 cm^{-1}), and the CH$_2$ wagging deformation (1212 cm^{-1}).[53]

Polymerization of Styrene and Methyl Methacrylate in the Presence of the Dendritic RAFT Agents. Kinetic studies were carried out for the polymerization of styrene and methyl methacrylate in the presence of the dendritic Gn-Cbz-CTA (n = 1–4) series as chain transfer agents. The polymerizations were carried out in benzene using AIBN as the initiator. Exploratory experiments were conducted to identify the opti-
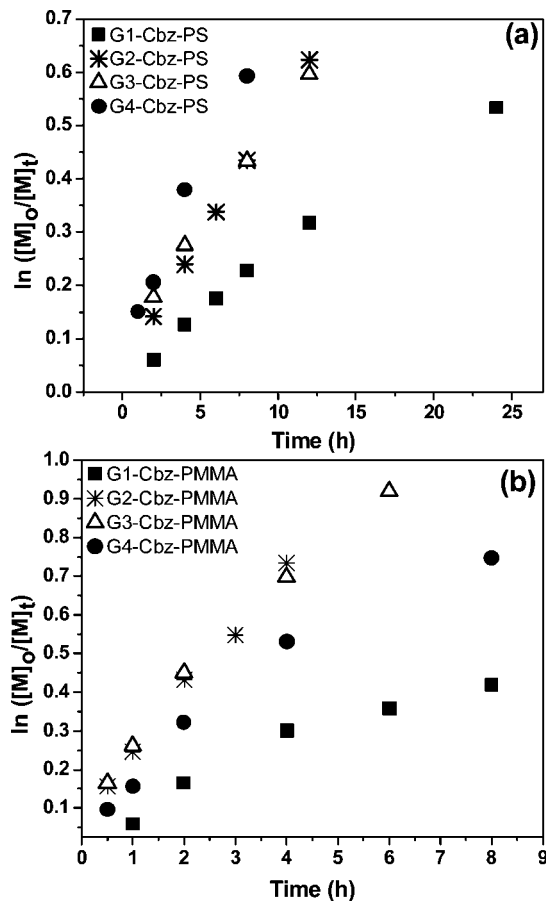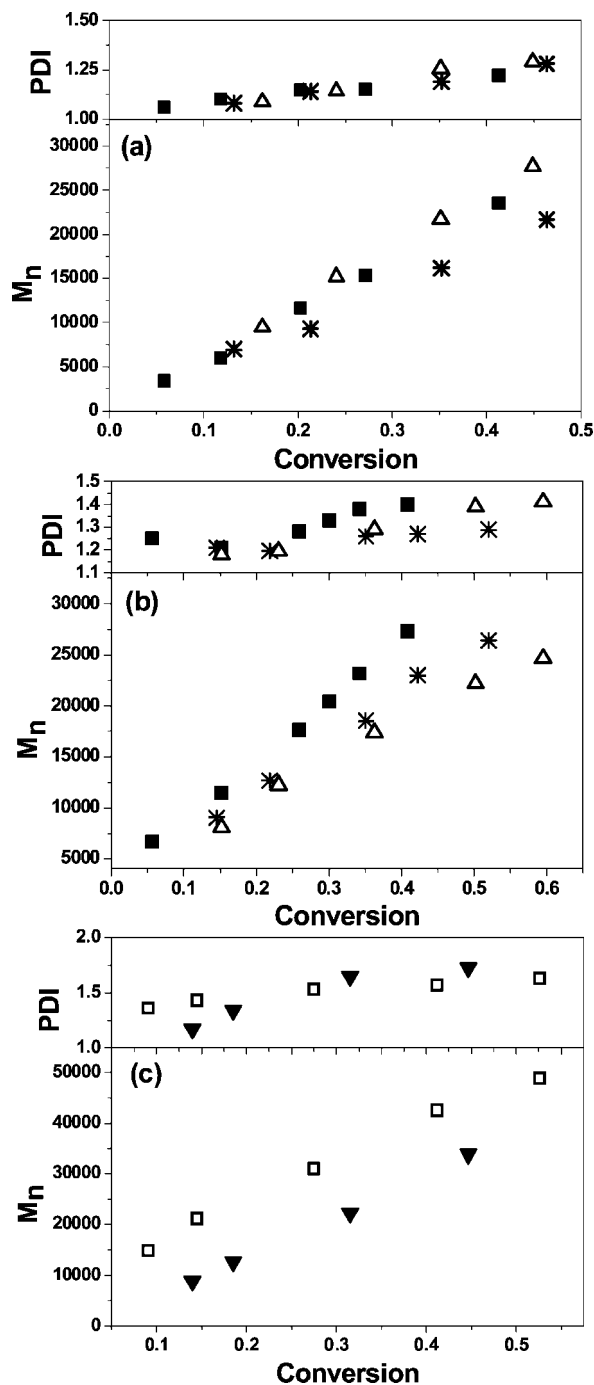

Figure 3. Kinetic plots for the polymerization of (a) styrene and (b) methyl methacrylate in the presence of the Gn-Cbz-CTA series.
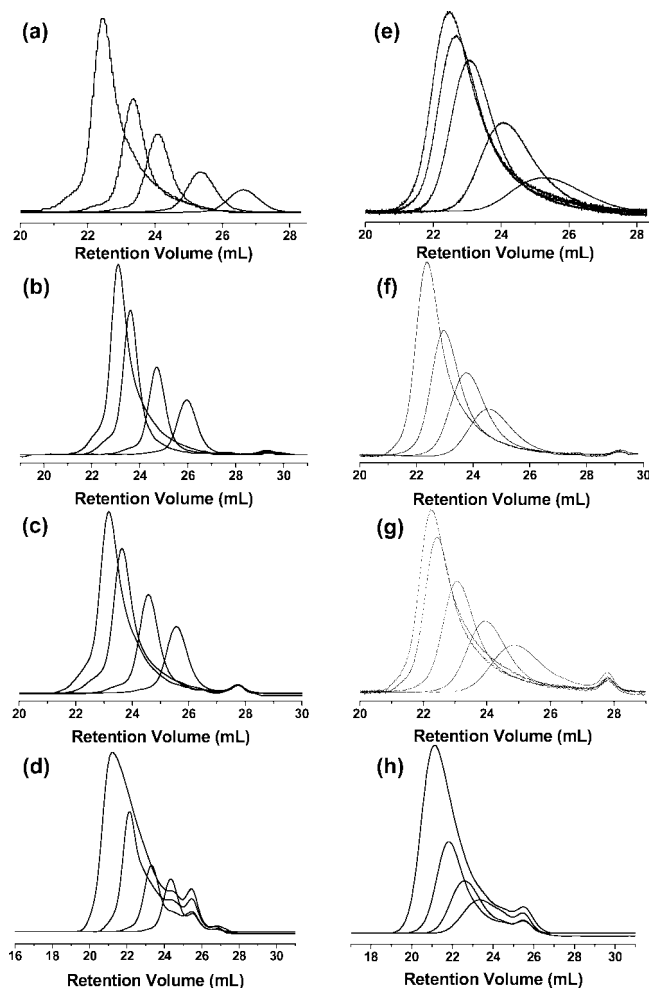
mum polymerization conditions for styrene and methyl methacrylate in the presence of the dendritic CTAs. For the G1-Cbz-CTA case, the following conditions were employed: (a) styrene–[M]:[CTA], 500:1; [CTA]:[I], 4:1; 70 °C; (b) MMA–[M]:[CTA], 600:1; [CTA]:[I], 1.6:1; 70 °C. In the case of G2-Cbz-CTA and G3-Cbz-CTA, the following conditions were found to yield optimal results: (a) styrene–[M]:[CTA], 500:1; [CTA]:[I], 3:1; 75 °C; (b) MMA–[M]:[CTA], 600:1; [CTA]:[I], 1.6:1; 80 °C. For G4-Cbz-CTA, the conditions were as follows: (a) styrene–[M]:[CTA], 1000:1; [CTA]:[I], 3:1; 75 °C; (b) MMA–[M]:[CTA], 1000:1; [CTA]:[I], 1.6:1; 75 °C. Aliquots collected over the course of the reaction were utilized to monitor the kinetic profile on the basis of monomer conversion vs time and to examine the evolution of molecular weight and polydispersity as a function of conversion. Figure 3a shows the pseudo-first-order kinetic plots for the polymerization of styrene in the presence of the dendritic CTAs. These plots indicate a constant radical concentration over the course of the reaction consistent with a well-controlled/living polymerization. Similar results were observed in the case of MMA (Figure 3b). As shown in Figure 3b, the kinetic plot for G1-Cbz-CTA/MMA deviates from linearity as the reaction proceeds, suggesting that the radical concentration in the reaction media is reduced. This observation is most likely attributed to undesirable side reactions and chain termination events. The observed increase in the overall rate of polymerization for G2- and G3-Cbz-CTA/styrene is attributed to the higher molar concentration of initiator (0.003 M for G2- and G3- and 0.0019 M for G1-Cbz-CTA) and the increased reaction temperature.

A similar increase in the rate of polymerization was observed for G2- and G3-Cbz-CTA/MMA and can be attributed to the increase in reaction temperature. Similarly, the higher rate of

Figure 4. Evolution of molecular weight and PDI with conversion for the polymerization of (a) styrene and (b) methyl methacrylate in the presence of the Gn-Cbz-CTA series (n = 1−3): G1 (■), G2 (∗), G3 (△), and (c) G4-Cbz-PS (▼) and G4-Cbz-PMMA (□).

Figure 5. Size exclusion chromatograms (crude reaction mixture) collected over time for the Gn-Cbz-CTA series. PS: (a) G1, (b) G2, (c) G3, (d) G4; PMMA: (e) G1, (f) G2, (g) G3, (h) G4.

polymerization for styrene in the presence of G4-Cbz-CTA (compared to G2 and G3) is attributed to the decreased CTA concentration. For G4-Cbz-CTA/MMA, a decrease in the rate of polymerization was observed in comparison with G2- and G3-Cbz-CTA. While a lower concentration of CTA was employed in the case of G4-Cbz-CTA/MMA, a slightly lower reaction temperature was also employed. It should be noted that there was no apparent dependence of the polymerization rate on the generation of the dendron under identical conditions for styrene and MMA (data not shown). The ability of the dendritic CTAs to control the molecular weight and give narrow polydispersities under the described conditions is evident in the M_n vs conversion plots shown in Figure 4a−c for styrene and MMA. As expected for a controlled/living process, the molecular

weights increase linearly with conversion in each case of the Gn-Cbz-CTA series for the range of conversions investigated in this study. The experimentally determined number-average molecular weights were found to be in reasonable agreement with the theoretical values calculated based on the observed conversion (refer to Tables 1 and 2), although in some cases the values determined from GPC were found to be lower than the theoretical prediction particularly as the generation of the dendron increases. This effect can be attributed to the difference in hydrodynamic volume of the hybrid dendritic−linear block copolymer and the linear standards used for calibration. This effect was particularly noticeable in the case of G2- and G4-Cbz-CTA/MMA where solution properties play a larger role due to the dissimilar block components.[22] Similar results have been reported by Gitsov et al.[26] and Leduc et al.[13] for similar linear−dendritic block copolymers. The evolution of molecular weight and polydispersity was followed by collecting aliquots of the reaction mixture over the course of the reaction. Unless otherwise noted, the GPC chromatograms represent results from the crude reaction mixture. However, the actual MW and PDI values were taken from purified polymer samples as discussed below. The GPC chromatograms for the Gn-Cbz-CTA (n = 1−4) series are shown in Figure 5a−d for PS and Figure 5e−g for PMMA. In each case for both styrene and MMA, a stepwise decrease in retention volume was observed as a function of reaction time. This behavior is consistent with a well-controlled or "living" polymerization. However, analysis of the crude polymerization mixtures of styrene and MMA for the second,
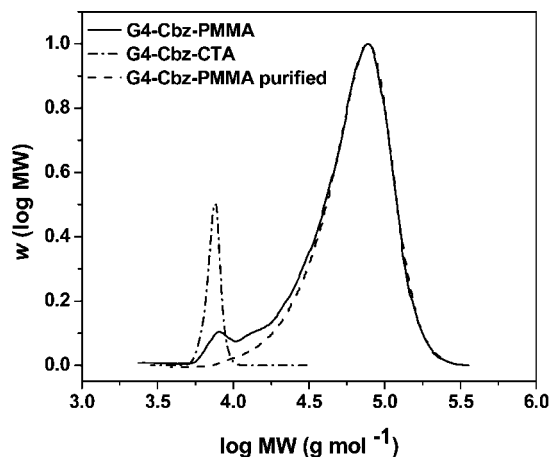
Figure 6. Size exclusion chromatograms of crude G4-Cbz-PMMA before (solid line) and after (dash line) purification. The dash-dotted line represents the pure G4-Cbz-CTA compound.

Figure 7. ¹H NMR spectra of (a) PMMA and (b) PS using G4-Cbz-CTA as a chain transfer agent.

third, and fourth generation CTAs revealed the presence of low molecular weight species with similar characteristics of the respective "starting" chain transfer agents.

As an example, the GPC chromatograms for pure G4-Cbz-CTA and crude G4-Cbz-PMMA are shown in Figure 6. The molecular weight of the dendritic impurity in the reaction mixture is very similar to that of the pure CTA. These impurities were observed at low conversions and are most likely the result of chain termination events after the addition of several monomer units. Similar results have been reported by Leduc and co-workers for both nitroxide-mediated and atom transfer radical polymerization using dendritic initiators.[13] Fortunately, these impurities did not appear to affect the course of the polymerization reaction and could easily be removed by precipitation or by passing through a short alumina column. The GPC chromatogram of G4-Cbz-PMMA before and after purification is shown in Figure 6, illustrating the complete removal of the dendritic impurity. The dendritic impurities seem to be more prevalent as the generation of the dendron increases, indicating the size, and perhaps the shape of the dendron, might influence the degree of termination events at low conversions. No such impurities could be observed for the first generation chain transfer agent. Further investigation is underway to identify and reduce these early termination events using dendritic CTAs. Namely, by introducing an additional spacer between the dendron and the active CTA portion of the molecule, it might be possible to avoid the presence of these impurities.

Structural Characterization. The structure of the dendritic−linear block copolymers was characterized by NMR, Raman, and FTIR spectroscopy, and the thermal properties were studied by thermogravimetric analysis (TGA) and differential scanning calorimetry (DSC). Figure 7 shows the representative ¹H NMR spectra of the (a) G4-Cbz-PMMA and (b) G4-Cbz-PS block copolymers. The spectra reveal several characteristic features for both the linear and dendritic blocks that are in good agreement with the expected structure. For G4-Cbz-PMMA, the characteristic resonances for the methyl and methylene protons are observed at chemical shifts of 0.90 and 1.70−2.01 ppm. Likewise, the resonances assigned to the aromatic and methylene protons of polystyrene are observed as broad peaks from $\delta \sim$ 6.3−7.3 and 1.23−2.0 ppm, respectively. The broad peaks of the polymers overlap many of the peaks associated with the dendritic fraction of the structure; however, those peaks that are distinguishable are labeled in accordance with the dendritic structure shown in Figure 2. The block copolymer structure was further confirmed by FTIR and Raman spectroscopy. Figure S2a (see Supporting Information) shows the (a) FTIR of a G3-Cbz-
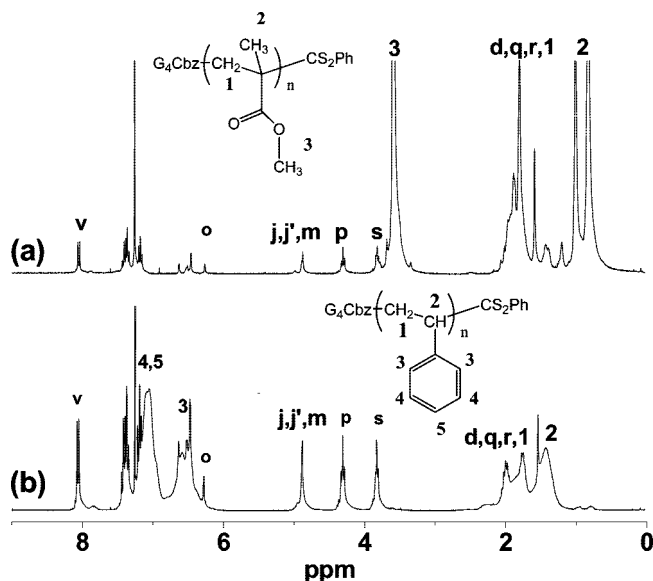
PMMA sample. The FTIR spectrum showed the characteristic absorption bands for the dendritic portion of the block copolymer at 3000−3100 cm⁻¹ for the aromatic C=H stretch and at 1597 cm⁻¹ for the aromatic C=C stretch. The strong absorption bands at 1732 and 1150 cm⁻¹ are assigned to the C=O stretch and the C=O=C stretch, respectively, and are attributable to the PMMA component of the structure. The aliphatic C=H stretch of the PMMA backbone and dendritic structure were also observed at 2800−2970 cm⁻¹. The Raman spectrum of G3-Cbz-PMMA shown in Figure S2b gives complementary information to identify the two block copolymer components. The overlapping bands at 1573−1624 and 1313−1346 cm⁻¹ were assigned to C=C stretch of benzene ring within the dendritic and carbazole structures. Bands assigned to the PMMA structure including the C=O, CH₃=O, and the C=O=C stretches were observed at 1728, 1450, and 810 cm⁻¹, respectively. Furthermore, the distinctive absorption bands attributable to the C=S stretch and the C−S stretch were observed at 1226 and 640 cm⁻¹, indicating that a large number of the block copolymer chains retain the RAFT active end group.

Thermal Properties of the Dendritic−Linear Block Copolymers. The thermal stability of the dendritic-linear block copolymers was assessed by TGA under a nitrogen atmosphere with a heating rate of 10 °C/min. The thermogravimetric profiles for the G*n*-Cbz-PS series (*n* = 1−4) are shown in Figure 8. The samples analyzed exhibited similar molecular weight characteristics as determined by SEC analysis. The overall molecular weight (M_n) of the samples ranged from approximately 6000 to 12 680 Da. As indicated in Figure 9, the decomposition of the block copolymers proceeds via a two-step process. The weight loss observed at an onset temperature of ∼238 °C can be attributed to the presence of the labile dithioester moiety at the chain end as a result of the RAFT-mediated polymerization.[54] The onset of weight loss for the major decomposition step was found to vary slightly depending on the generation of the dendritic component. The onset temperature was observed at 378, 381, 380, and 388 °C for G1-Cbz-PS (sample 1b), G2-Cbz-PS (sample 2b), G3-Cbz-PS (sample 3a), and G4-Cbz-PS (sample 4b) block copolymers, respectively. In addition, an enhancement in the thermal properties of the block copolymers with increasing generation number was indicated by observing the temperature at 50% mass loss. This value increased from 405 °C for G1-Cbz-PS, 412 °C
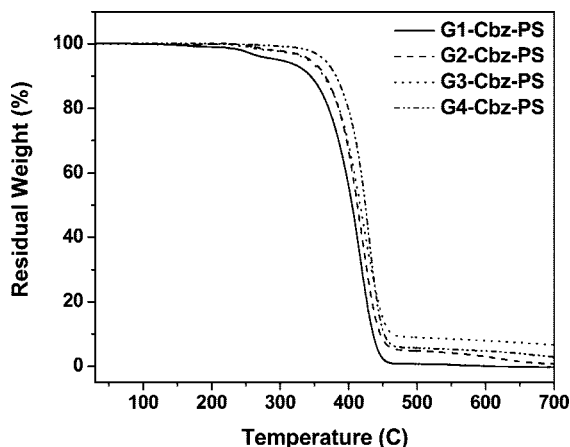
Figure 8. Thermogravimetric profiles for the G*n*-Cbz-PS series (*n* = 1−4) under a N$_2$ atmosphere at 10 °C/min: (—) 1b, G1-Cbz-PS; (---) 2b, G2-Cbz-PS; (•••) 3a, G3-Cbz-PS; (− •• −) 4b, G4-Cbz-PS.
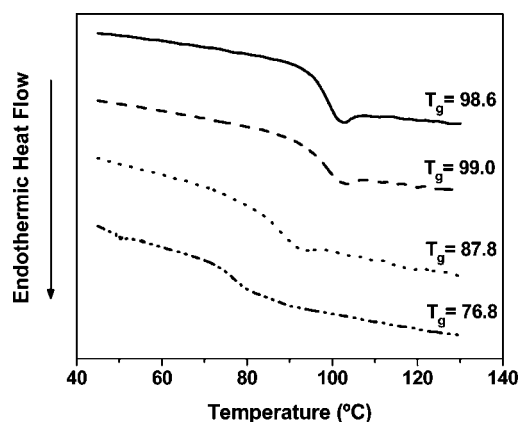
Figure 9. DSC traces (vertically shifted for clarity) of the G*n*-Cbz-PS block copolymer series: (—) 1e, G1-Cbz-PS; (---) 2d, G2-Cbz-PS; (•••) 3c, G3-Cbz-PS; (− •• −) 4c, G4-Cbz-PS.

for G2-Cbz-PS, 417 °C for G3-Cbz-PS, to 424 °C for G4-Cbz-PS.

These results indicate the larger generation dendritic block imparts a slightly greater thermal stability to the block copolymer structure. The current results are contrary to those reported by Jiang et al. for similar dendritic−linear systems.[17,55] However, it is not clear as to the compositions (weight fraction and molecular weight) of the block copolymer utilized for the thermal analysis in their publications. Thus, a direct comparison is not possible with the present results.

The DSC traces for the G*n*-Cbz-PS series (*M*$_n$ ranging from 21 600 to 22 500) of block copolymers are shown in Figure 9. Consistent with results on similar dendritic−linear systems, a single glass transition temperature (*T*$_g$) was observed for each block copolymer regardless of the dendron generation or overall composition, indicating a high degree of compatibility between the block components.

This was also the observation for the G*n*-Cbz-PMMA series. In the present case, the *T*$_g$ for the lower generation (G$_1$, 98.6 °C; G$_2$, 99.0 °C) block copolymers was essentially unchanged with increasing generation. However, the *T*$_g$ for G3-Cbz-PS and G4-Cbz-PS was broadened and shifted to substantially lower temperatures of 87.8 and 76.8 °C, respectively. Although the overall molecular weight characteristics are similar, the trend appears to be closely related to weight fraction of the constituent polymers. As the weight fraction of the linear PS decreased, a corresponding decrease in the *T*$_g$ of the block copolymer was observed. Indeed, the experimental *T*$_g$ values observed for the

dendritic−linear block copolymers were found to be in good agreement with those calculated using the Fox equation; the predicted *T*$_g$ is dependent only on the fractional weight composition and the experimentally determined glass transition temperatures of the constituent polymers.[56] While *T*$_g$ is closely related to molecular weight and the rigidity of the polymer backbone, the heat capacity (ΔC_p) is linked to the macromolecules' vibrational and conformational degrees of freedom. Interestingly, the evolution of the heat capacity exhibited a generation-dependent trend similar to the *T*$_g$. The ΔC_p values showed a systematic decrease from 0.339, 0.332, 0.329, to 0.255 J (g °C)$^{-1}$ for G1-, G2-, G3-, and G4-Cbz-PS, respectively. These results show that the generation of the dendritic block plays an important role in the overall mobility of the dendritic−linear block copolymers in the solid state. A similar trend in heat capacities was reported by Dantras and co-workers for their phosphorus-containing dendrimers in which the global molecular motion was reduced as the generation number increased.[57] Undoubtedly, the thermal transitions for the dendritic−linear block copolymers reported in the present study are the result of a complex interplay between the properties of the linear and dendritic components. A thorough understanding of this relationship will be crucial for the development application specific dendritic−linear block copolymer systems.

Electrodeposition. By design, the dendritic−linear block copolymer is essentially an electrochemically active macromonomer by virtue of the carbazole groups available for electropolymerization or electrochemical cross-linking to form thin films. In principle, the properties can vary with generation of the dendron as well as the solution properties of the linear block. In this case, these properties were monitored primarily with the G-4 derivatives leaving the G-1−G-3 derivatives subject to further study.

Electrochemical Quartz Crystal Microbalance Analysis. Electrochemical quartz crystal microbalance is an exceptionally versatile technique for in situ monitoring of gravimetric changes occurring at electrode surfaces.[58,59] The change in mass (Δm) is related to the change in the fundamental resonance frequency ΔF (Hz) of the QCM crystal by the well-known Sauerbrey equation:[60]

$$\Delta F = \frac{-2F_q^2}{A_e\sqrt{\rho_q\mu_q}}\Delta m \qquad (1)$$

where F_q is the fundamental resonant frequency of the QCM (5 MHz), A_e is the area of the electrode (1.327 cm^2), ρ_q is the density of the quartz (2.65 g/cm^3), and μ_q is the shear modulus of the quartz (2.95 × 10^6 N/cm^2). For the Sauerbrey equation to be valid, the adsorbed film is assumed to possess the same acoustic−elastic properties as the quartz resonator. If the adsorbed film thickness is small in comparison with the thickness of the crystal and if the ΔF is much smaller than the resonant frequency of the bare crystal, this rigid model approximation is applicable. Furthermore, the mass sensitivity has previously been shown to be approximately the same for liquid and air/vacuum measurements, yielding the ability to accurately monitor changes in mass adsorbed from solution.[61] However, an adsorbed viscoelastic overlayer in the case of viscous liquids and some polymer thin films results in a viscous coupling of the solution or film to the crystal, effectively adding a mass component to the oscillating crystal. Thus, the resulting resonant frequency change is more complex and was first described by Kanazawa et al.[62] as follows:

$$\Delta F = -F_q^{3/2}\sqrt{\frac{\eta_L\rho_L}{\pi\mu_q\rho_q}} \qquad (2)$$

where F_q is the resonant frequency of unloaded crystal in Hz, ρ_q is the density of quartz (2.648 × 10^3 kg/m^3), μ_q is the shear

modulus of quartz $(2.947 \times 10^{10}$ Pa$)$, ρ_L is the liquid density (kg/m^3), and η_L is the liquid viscosity in contact with electrode in N s/m^2. Hence, when the QCM operates under inelastic conditions, it becomes difficult to differentiate contributions attributed to the bound mass from that of the solution viscosity to the total change in frequency. In this case, impedance analysis of the QCM resonator has proven to be effective in providing additional information on the solid/liquid interface.[62,63] This analysis is based on the well-known Butterworth−van Dyke (B−VD) equivalent circuit that provides the structure for relating the electrical properties of the quartz resonator to the mechanical properties of the deposited film.[59] In this regard, the B−VD circuit element R (motional resistance) is useful in probing the energy loss or dissipation factor (D) due to the damping process that occurs in viscoelastic systems. The relationship between ΔR and ΔF under liquid loading is given by the equation[64]

$$\Delta R = (2\pi F \rho_L \eta_L)^{1/2} A_r / k^2 \qquad (3)$$

where ΔR is the change in resonance resistance in Ω, A_r is the active crystal area, and k is the electromechanical coupling factor. Thus, a large increase in ΔR is correlated with an increase in the viscoelasticity of the layer adjacent to the crystal surface while a small change in ΔR is indicative of a more rigid adsorbed layer. Of course, if $\Delta R = 0$, then the original Sauerbrey equation is valid. So, monitoring the change in the resonance resistance $(\Delta R \ (\Omega))$ as a function of frequency shift, in some cases, provides a means to quantitatively determine the shear viscosity and elastic modulus of films and in others a means for qualitatively comparing various thin film systems.

Here, E-QCM was performed to simultaneously monitor the change in mass and resonance resistance at the working electrode during the electrochemical deposition of the dendritic−linear block copolymers. A 5 MHz AT-cut Au-coated quartz crystal with an effective area of 1.327 cm^2 was used as the working electrode. Cyclic voltammetry was utilized to study the electrochemical behavior of the carbazole-modified dendritic−linear block copolymers as deposited from solution during the E-QCM experiments. Figure 10 shows the cyclic voltammograms (CV) of G4-Cbz-PS (a) and G4-Cbz-PMMA (b) deposited from a 0.1 M TBAH/CH$_2$Cl$_2$ (scan rate 20 mV s^{-1}) solution. In the first cycle, the onset of oxidation of the peripheral carbazole monomers was observed at ∼1.1 V with the corresponding reduction peak maximum occurring at ∼1.2 V for the G4-Cbz PS and G4-Cbz-PMMA systems. This is accompanied by the formation of the first layer of a conjugated network film (discussed further in the next section). In addition, a second redox peak maximum was observed at a lower potential in the return scan of the first cycle (∼0.8 V). Subsequent cycles show further deposition of the electroactive block copolymer at a similar onset potential with an additional oxidation peak maxima observed in the ranges of 0.82−0.88 and 0.78−0.84 V (doping) and the corresponding reduction peak maxima at 0.79−0.82 and 0.77−0.80 V (dedoping) for G4-Cbz-PS and G4-Cbz-PMMA, respectively. The presence of the two redox processes in these systems possibly indicates the presence of both 3,6- and 2,7 linkages in the conjugated polycarbazole network.[65] Figure S3 (Supporting Information) illustrates schematically the radical cation coupling mechanism between carbazole groups during the electrochemical deposition and polymerization, leading to cross-linked dendrons at the electrode substrate.[49]

In lieu of a more rigorous quantitative treatment, the behavior of mass transport and viscoelastic properties in terms of the relationship between ΔF and ΔR of the block copolymer thin films is discussed in a qualitative sense for comparative purposes. Figure 11 shows the frequency shift and change in resonance resistance as a function of time during the electropo-
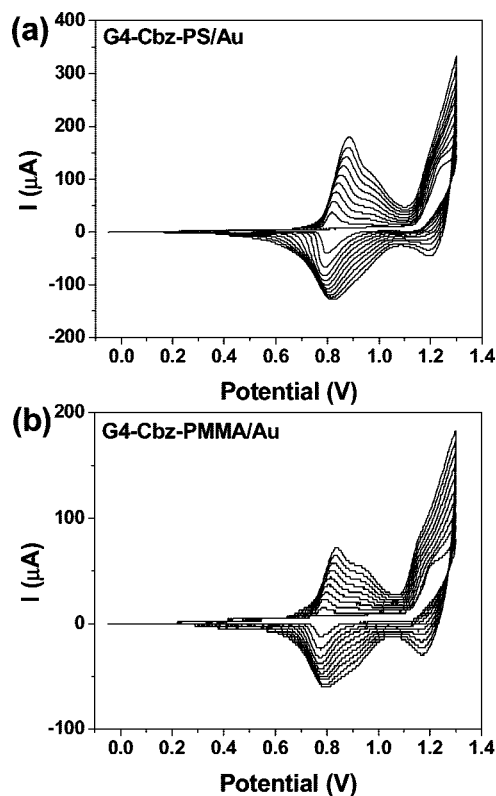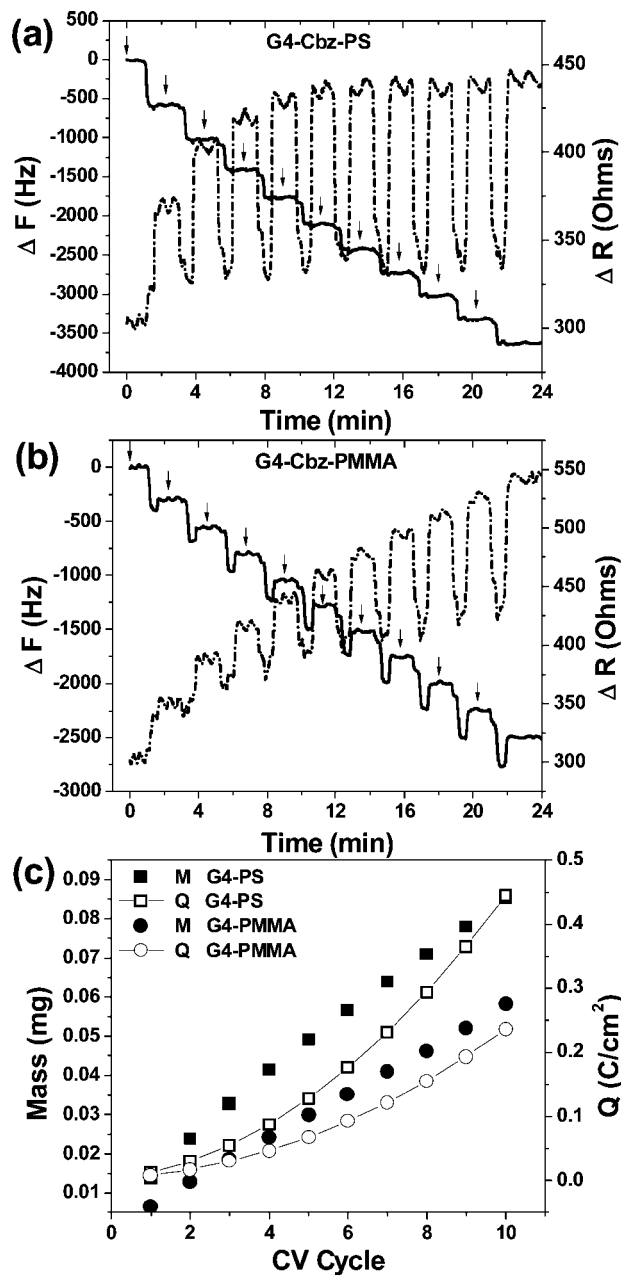

Figure 10. CV for the electrochemical deposition of G4-Cbz-PS (a) and G4-Cbz-PMMA (b) on Au at a scan rate of 20 mV/s. The cyclic voltammograms on Au were obtained from electrochemical QCM experiments.

lymerization of (a) G4-Cbz-PS and (b) G4-Cbz-PMMA, respectively, by cycling the potential between −0.05 and 1.3 V. The arrows indicate the beginning of each potential cycle. The mass of the polymer deposited on the working electrode was linear as a function of CV cycle with a corresponding increase in the amount of charge indicative of the growth of an electrochemically active thin film as shown in Figure 11c.
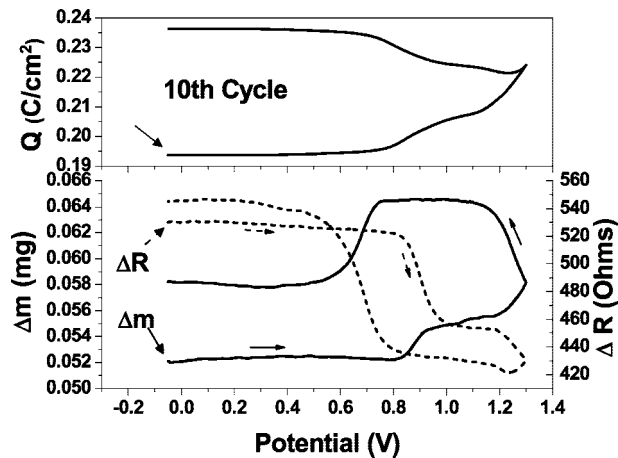
The growth of the G4-Cbz-PS film thickness occurs at a faster rate than the G4-Cbz-PMMA system and results in a higher thickness at the end of the 10th potential cycle. This observation was confirmed by ellipsometry measurements giving a dry film thickness of 111 and 89.8 nm for G4-Cbz-PS and G4-Cbz-PMMA, respectively. In each case, a complex stepwise response in the frequency and resonance resistance was observed with each potential cycle, indicating processes related to the deposition, doping, and dedoping of the polymer film. In the first cycle, a continuous decrease in ΔF was observed over the potential range for the oxidation (1.2−1.3 V, anodic scan) and reduction (1.3−1.1 V, cathodic scan) of the carbazole monomers (1.1−1.3 V), indicating the deposition of a thin film of conjugated polymer occurs within this range. A simultaneous increase in ΔR was observed with the decrease in ΔF, further indicating the film deposition process. At the potential corresponding to the second redox process (∼0.8 V) on the cathodic scan of the first cycle, an increase in ΔF was observed, indicating a mass loss due to the expulsion of anions from the film. With increasing CV cycles, the ΔF and particularly the ΔR response resulting from the deposition, doping, and dedoping processes become more prominent. This observation is shown in greater detail by examining the change in mass (Δm) and ΔR response as a function of applied potential.

For example, the 10th cycle of the G4-Cbz-PMMA system is shown in Figure 12. The change in mass is constant for the anodic scan up to a potential of 0.8 V. At this point, the onset

Figure 12. Change in mass and resonance resistance (ΔR) as a function of potential for G4-Cbz-PMMA monitored by E-QCM. The data shown is for the 10th CV cycle and is representative of the previous cycles differing only in the magnitude of each response (2−9). The upper figure correlated the amount of charge to the change in mass as a function of potential.

Figure 13. Change in resonance resistance vs the change in frequency for the CV deposition of (■) G4-Cbz-PS and (○) G4-Cbz-PMMA.
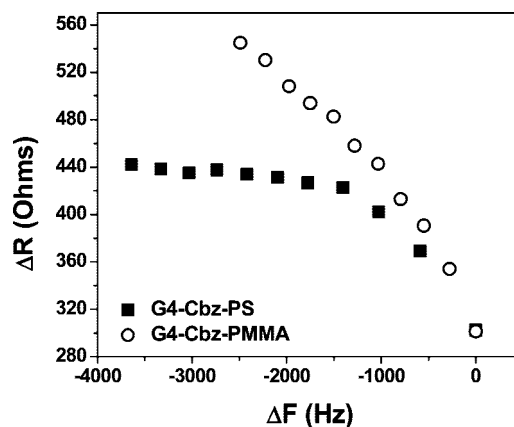

Figure 11. Electrochemical QCM for the G4-dendritic linear block copolymers at a scan rate of 20 mV/s: Δfrequency (—) and Δresistance (- · -) vs time for (a) G4-Cbz-PS and (b) G4-Cbz-PMMA (c). The mass and charge vs the number of CV cycles for the G4-Cbz block copolymers indicating a linear deposition.

of mass transport was observed with a sharp increase from 0.8 to 1.0 V which is correlated to the injection of anions into the film upon doping. This result is supported by the simultaneous increase in charge over this potential range. It should be noted that this mass increase was not observed in the initial cycle due to the absence of doping. A second regime in mass change was observed from ∼1.1 to 1.3 V in the anodic scan and from 1.3 to 1.1 V in the cathodic scan, which is mostly due to the oxidation of the peripheral-carbazole monomers to form a more conjugated polymer network, while the overall increase in mass is a combination of both doping and polymer deposition. The ejection of anions from the film (dedoping) was observed by a corresponding decrease in mass at potentials from ∼0.8 to 0.5 V in the cathodic scan. Interestingly, the ΔR value substantially decreases upon doping of the polymer film and deposition process. As can be seen in Figure 12, the change in resonance

resistance occurs in two regimes with the initial and most prominent decrease (60 Ω) corresponding to the doping process and the second attributed to a combination of doping and film deposition (35 Ω). Likewise, a substantial increase in ΔR (125 Ω) at 0.8 V in the cathodic scan is correlated with dedoping and expulsion of the anions from the film. These results suggest that the film becomes more rigid upon inclusion of anions in the film during the doping process, and viscoelasticity is recovered upon dedoping. This observation might be the attributed to a decrease in free volume within the block copolymer thin film upon inclusion of the supporting electrolyte anions leading to a more rigid mechanical response.

Furthermore, we observed significant differences in the viscoelastic response between the PMMA and PS systems, indicating the linear component plays an important role in the viscoelasticity of the film. Referring back to Figure 11a,b, the overall change in ΔR for the G4-Cbz-PS (∼192 Ω) and the G4-Cbz-PMMA (∼246 Ω) indicates the resulting film containing PMMA is more viscoelastic under the current experimental conditions. Figure 13 shows the relationship between ΔR and ΔF for the G4-Cbz-PS and G4-Cbz-PMMA plotted in the dedoped state at the end of each potential cycle (0 V). Interestingly, the G4-Cbz-PS system shows an initial response in ΔR as a function of mass but quickly plateaus after the fourth potential cycle, becoming essentially independent of the total amount of mass deposited. On the other hand, the G4-Cbz-

PMMA system shows a continued dependence of ΔR on ΔF up to 10 potential cycles. At this point, it is difficult to discern the contributions to ΔR from each block component in relation to the overall block copolymer composition. Further investigation is required and is underway to study the effect of block copolymer composition, degree of polymerization, and dendron generation on the viscoelastic and electrochemical behavior of the hybrid thin films. In the future, investigations on targeted electrodeposition parameters will be made to obtain "polymer brush" type of electrochemical grafting conditions. The electrochemical behavior of the corresponding cross-linked dendrimers has recently been reported by our group.[49]

Conclusions

This work has demonstrated a first example of electrochemically active functional dendritic−linear block copolymers prepared by RAFT polymerization. A series of carbazole-functionalized dendritic chain transfer agents were synthesized and successfully utilized in the preparation of dendritic−linear block copolymers comprised of either poly(styrene) or poly-(methyl methacrylate) as the linear block. The polymerization of these monomers in the presence of the dendritic CTAs showed characteristics of a well-controlled or "living" radical polymerization affording good control over the molecular weight and polydispersity of the linear block. The generation of the dendritic CTA played an important role in the termination processes in the early stages of the reaction. The thermal properties of the functional block copolymers were studied and found to be dependent on both the generation number of the dendron and the fractional weight composition. A slight enhancement in the thermal degradation was observed with increasing generation. The T_g and ΔC_p exhibited trends with regard to the generation number as well; a decrease in the T_g and ΔC_p was observed with increasing generation for polymers of similar MW characteristics, indicating the unique properties of these hybrid materials. In addition, we have demonstrated the electrochemical deposition of block copolymer thin films via the electropolymerization (cross-linking) of the carbazole monomers at the periphery of the dendritic block utilizing the "precursor polymer" approach. The deposition kinetics and viscoelastic properties of the deposited materials were studied in situ using E-QCM. The cross-linked polymer films showed differences in both the viscoelasticity and morphology as a result of different chemical compositions. The development and incorporation of electroactive and optical properties into these unique block copolymer systems and their resulting mesophases might have significant implications in the study of nanostructured materials and their role in mediating electron and charge carrier transport. The design and characterization of these unique systems is an ongoing process in our laboratory. In addition, future investigations will be made toward "polymer brush" type of electrochemical grafting conditions.

Supporting Information Available: NMR characterization and FT-IR and Raman spectroscopy of the CTAs and the dendron−linear polymers. This material is available free of charge via the Internet at http://pubs.acs.org.

References and Notes

(1) Newkome, G. R.; Moorefield, C. N.; Vögtle, F. *Dendritic Molecules: Concepts, Syntheses, Perspectives*; VCH: Weinheim, 1996.

(2) Hahn, U.; Gorka, M.; Vögtle, F.; Vicinelli, V.; Ceroni, P.; Maestri, M.; Balzani, V. *Angew. Chem., Int. Ed.* **2002**, *41*, 3595.

(3) Chen, H. T.; Neerman, M. F.; Parrish, A. R.; Simanek, E. E. *J. Am. Chem. Soc.* **2004**, *126*, 10044.

(4) Murugan, E.; Sherman, R. L.; Spivey, H. O.; Ford, W. T. *Langmuir* **2004**, *20*, 8307.

(5) Gittins, P. J.; Twyman, L. J. *J. Am. Chem. Soc.* **2005**, *127*, 1646.

(6) Percec, V.; Cho, W. D.; Ungar, G. *J. Am. Chem. Soc.* **2000**, *122*, 10273.

(7) Patton, D.; Park, M. K.; Wang, S.; Advincula, R. C. *Langmuir* **2002**, *18*, 1688.

(8) Deng, S.; Locklin, J.; Patton, D.; Baba, A.; Advincula, R. C. *J. Am. Chem. Soc.* **2005**, *127*, 1744.

(9) Newkome, G. R.; Baker, G. R.; Arai, S.; Saunders, M. J.; Russo, P. S.; Theriot, K. J.; Moorefield, C. N.; Rogers, L. E.; Miller, J. E.; Lieux, T. R.; Murray, M. E.; Phillips, B.; Pascal, L. *J. Am. Chem. Soc.* **1990**, *112*, 8458.

(10) Gitsov, I.; Wooley, K. L.; Frechet, J. M. J. *Angew. Chem., Int. Ed. Engl.* **1992**, *31*, 1200.

(11) Chapman, T. M.; Hillyer, G. L.; Mahan, E. J.; Shaffer, K. A. *J. Am. Chem. Soc.* **1994**, *116*, 11195.

(12) Van hest, J. C. M.; Delnoye, D. A. P.; Baars, M.; Vangenderen, M. H. P.; Meijer, E. W. *Science* **1995**, *268*, 1592.

(13) Leduc, M. R.; Hawker, C. J.; Dao, J.; Frechet, J. M. J. *J. Am. Chem. Soc.* **1996**, *118*, 11111.

(14) Iyer, J.; Fleming, K.; Hammond, P. T. *Macromolecules* **1998**, *31*, 8757.

(15) Zubarev, E. R.; Stupp, S. I. *J. Am. Chem. Soc.* **2002**, *124*, 5762.

(16) Johnson, M. A.; Iyer, J.; Hammond, P. T. *Macromolecules* **2004**, *37*, 2490.

(17) Jiang, G.; Wang, L.; Chen, T.; Wang, J.; Chen, C.; Yu, H. *J. Appl. Polym. Sci.* **2005**, *98*, 1106.

(18) Cho, B. K.; Jain, A.; Gruner, S. M.; Wiesner, U. *Science* **2004**, *305*, 1598.

(19) Pochan, D. J.; Pakstis, L.; Huang, E.; Hawker, C.; Vestberg, R.; Pople, J. *Macromolecules* **2002**, *35*, 9239–9242.

(20) Santini, C.; Johnson, M.; Boedicker, J.; Hatton, T.; Hammond, P. *J. Polym. Sci., Part A: Polym. Chem.* **2004**, *42*, 2784–2814.

(21) Mackay, M. E.; Hong, Y.; Jeong, M.; Tande, B. M.; Wagner, N. J.; Hong, S.; Gido, S. P.; Vestberg, R.; Hawker, C. J. *Macromolecules* **2002**, *35*, 8391–8399.

(22) Gitsov, I.; Frechet, J. M. J. *Macromolecules* **1993**, *26*, 6536.

(23) Aoi, K.; Motoda, A.; Okada, M.; Imae, T. *Macromol. Rapid Commun.* **1997**, *18*, 945.

(24) Passeno, L. M.; Mackay, M. E.; Baker, G. L.; Vestberg, R.; Hawker, C. J. *Macromolecules* **2006**, *39*, 740.

(25) Gitsov, I.; Wooley, K. L.; Hawker, C. J.; Ivanova, P. T.; Frechet, J. M. J. *Macromolecules* **1993**, *26*, 5621.

(26) Gitsov, I.; Frechet, J. M. J. *Macromolecules* **1994**, *27*, 7309.

(27) Van hest, J. C. M.; Baars, M.; Elissenroman, C.; Vangenderen, M. H. P.; Meijer, E. W. *Macromolecules* **1995**, *28*, 6689.

(28) Namazi, H.; Adeli, M. *J. Polym. Sci., A: Polym. Chem.* **2005**, *43*, 28.

(29) Gitsov, I.; Ivanova, P. T.; Frechet, J. M. J. *Macromol. Rapid Commun.* **1994**, *15*, 387.

(30) Al-Muallem, H. A.; Knauss, D. M. *J. Polym. Sci., Part A: Polym. Chem.* **2001**, *39*, 152.

(31) Knauss, D. M.; Al-Muallem, H. A. *J. Polym. Sci., Part A: Polym. Chem.* **2000**, *38*, 4289.

(32) Matyjaszewski, K.; Xia, J. H. *Chem. Rev.* **2001**, *101*, 2921.

(33) Chiefari, J.; Chong, Y.; Ercole, F.; Krstina, J.; Jeffery, J.; Le, T.; Mayadunne, R.; Meijs, G.; Moad, C.; Moad, G.; Rizzardo, E.; Thang, S. *Macromolecules* **1998**, *31*, 5559.

(34) Moad, G.; Rizzardo, E.; Thang, S. H. *Aust. J. Chem.* **2005**, *58*, 379.

(35) Leduc, M. R.; Hayes, W.; Frechet, J. M. J. *J. Polym. Sci., Part A: Polym. Chem.* **1998**, *36*, 1.

(36) Zhu, L. Y.; Tong, X. F.; Li, M. Z.; Wang, E. J. *J. Polym. Sci., Part A: Polym. Chem.* **2000**, *38*, 4282.

(37) (a) Zhao, Y. L.; Jiang, J.; Liu, H. W.; Chen, C. F.; Xi, F. *J. Polym. Sci., Part A: Polym. Chem.* **2001**, *39*, 3960. (b) Zhao, Y. L.; Jiang, J.; Chen, C. F.; Xi, F. *Polym. Int.* **2002**, *51*, 1334.

(38) Ge, Z.; Luo, S.; Liu, S. *J. Polym. Sci., Part A: Polym. Chem.* **2006**, *44*, 1357.

(39) Hao, X. J.; Malmstrom, E.; Davis, T. P.; Stenzel, M. H.; Barner-Kowollik, C. *Aust. J. Chem.* **2005**, *58*, 483.

(40) Zheng, Q.; Pan, C. Y. *Macromolecules* **2005**, *38*, 6841.

(41) Hong, C.; You, Y.; Liu, J.; Pan, C. *J. Polym. Sci., Part A: Polym. Chem.* **2005**, *43*, 6379.

(42) Xia, C.; Advincula, R. C.; Baba, A.; Knoll, W. *Chem. Mater.* **2004**, *16*, 2852.

(43) Deng, S.; Advincula, R. C. *Chem. Mater.* **2002**, *14*, 4073.

(44) Taranekar, P.; Fan, X.; Advincula, R. *Langmuir* **2002**, *18*, 7943.

(45) Baba, A.; Onishi, K.; Knoll, W.; Advincula, R. C. *J. Phys. Chem. B* **2004**, *108*, 18949.

(46) Taranekar, P.; Baba, A.; Fulghum, T. M.; Advincula, R. *Macromolecules* **2005**, *38*, 3679.

(47) Thang, S. H.; Chong, Y.; Mayadunne, R.; Moad, G.; Rizzardo, E. *Tetrahedron Lett.* **1999**, *40*, 2435.

(48) Patton, D. L.; Advincula, R. C. *Macromolecules* **2006**, *39*, 8674–8683.

(49) Taranekar, P.; Fulghum, T.; Patton, D.; Ponnapati, R.; Clyde, G.; Advincula, R. *J. Am. Chem. Soc.* **2007**, *129*, 12537–12548.

(50) Chong, Y. K.; Krstina, J.; Le, T. P. T.; Moad, G.; Postma, A.; Rizzardo, E.; Thang, S. H. *Macromolecules* **2003**, *36*, 2256.

(51) tenCate, M. G. J.; Rettig, H.; Bernhardt, K.; Borner, H. G. *Macromolecules* **2005**, *38*, 10643.

(52) Sarac, A.; Tofail, S.; Serantoni, M.; Henry, J.; Cunnane, V.; Mc-Monagle, J. *Appl. Surf. Sci.* **2004**, *222*, 148.

(53) Zhang, L.; Huo, F.; Wang, Z.; Wu, L.; Zhang, X.; Hoppener, S.; Chi, L.; Fuchs, H.; Zhao, J.; Niu, L.; Dong, S. *Langmuir* **2000**, *16*, 3813–3817.

(54) Patton, D. L.; Mullings, M.; Fulghum, T.; Advincula, R. C. *Macromolecules* **2005**, *38*, 8597.

(55) Jiang, G.; Wang, L.; Chen, T.; Yu, H. *Polymer* **2005**, *46*, 81.

(56) Fox, T. G. *Bull. Am. Phys. Soc.* **1956**, *1*, 123.

(57) Dantras, E.; Dandurand, J.; Lacabanne, C.; Caminade, A. M.; Majoral, J. P. *Macromolecules* **2002**, *35*, 2090.

(58) Abruña, H. D. *Electrochemical Interfaces: Modern Techniques for In-Situ Interface Characterization*; VCH Pub.: New York, 1991.

(59) Buttry, D. A.; Ward, M. D. *Chem. Rev.* **1992**, *92*, 1355.

(60) Sauerbrey, G. *Z. Phys.* **1959**, *155*, 206.

(61) Ward, M. D.; Buttry, D. A. *Science* **1990**, *249*, 1000.

(62) Kanazawa, K. *Faraday Discuss.* **1997**, *107*, 77.

(63) Etchenique, R.; Weisz, A. *J. Appl. Phys.* **1999**, *86*, 1994.

(64) Muramatsu, H.; Tamiya, E.; Karube, I. *Anal. Chem.* **1988**, *60*, 2142.

(65) Iraqi, A.; Wataru, I. *Chem. Mater.* **2004**, *16*, 442.

(66) Zhao, B.; Haasch, R. T.; MacLaren, S. *J. Am. Chem. Soc.* **2004**, *126*, 6124.

(67) Zhao, B.; Brittain, W. J. *J. Am. Chem. Soc.* **1999**, *121*, 3557.